FRI SAMPLING AND TIME-VARYING PULSES: SOME THEORY AND FOUR SHORT STORIES

Ayush Bhandari[†] *and Thierry Blu*[◇]

[†]Media Laboratory, Massachusetts Institute of Technology, Cambridge, MA, USA.

[◇]Department of Electronic Engineering, The Chinese University of Hong Kong, Shatin, Hong Kong.

Email: ayush@MIT.edu • thierry.blu@m4x.org

ABSTRACT

The field of signal processing is replete with exemplary problems where the measurements amount to time-delayed and amplitude scaled echoes of some template function or a pulse. When the inter-pulse spacing is favorable, something as primitive as a matched filter serves the purpose of identifying time-delays and amplitudes. When the inter-pulse spacing poses an algorithmic challenge, high-resolution methods such as finite-rate-of-innovation (FRI) may be used. However, in many practical cases of interest, the template function may be distorted due to physical properties of propagation and transmission. Such cases can not be handled well by existing signal models. Inspired by problems in spectroscopy, radar, photoacoustic imaging and ultra-wide band arrays, on which we base our case studies, in this work we take a step towards recovering spikes from time-varying pulses. To this end, we re-purpose the FRI method and extend its utility to the case of phase distorted pulses. Application of our algorithm on the above-mentioned case studies results in substantial improvement in peak-signal-to-noise ratio, thus promising interesting future directions.

Index Terms— Finite-rate-of-innovation, sparsity, spectral estimation, template matching, time-varying pulses.

1. INTRODUCTION

One signal model that is frequently encountered across various disciplines of science and engineering assumes form of,

$$y(t) = \sum\nolimits_{k=0}^{K-1} c_k \varphi(t - t_k) \equiv (\varphi * s)(t), \tag{1}$$

where s is a K-sparse signal and $\varphi(t)$ is a low-pass filter or template. Given equidistant samples $y_n = \{y(n\Delta)\}_{n=0}^{N-1}$ with sampling rate $\Delta > 0$, estimating s is a recurrent problem in time-delay estimation [1], resolution of echoes [2,3], sparse deconvolution [4] and super-resolution [5]. In the context of sampling theory, Vetterli, Blu and co-workers [6,7] have demonstrated that a continuous time sparse signal, which is completely characterized by $2K$ real-vaued unknowns $\{c_k, t_k\}_{k=0}^{K-1}$, can be uniquely recovered from $N \geq 2\Omega + 1$ samples provided that the the maximum frequency of φ satisfies $\Omega \geq K$. Under the framework of finite–rate–of–innovation (FRI) model [6], that is, signals that can be specified by countable degrees of freedom, these results have been extended far and wide [8–16]. FRI signals can broadly be studied in form of a generalized signal model,

$$y(t) = (\varphi * \mathcal{L}[s])(t), \qquad s(t) = \sum\nolimits_{k=0}^{K-1} c_k \delta(t - t_k), \tag{2}$$

This work was partly supported by a grant #CUHK14600615 from the Hong Kong Research Grants Council.

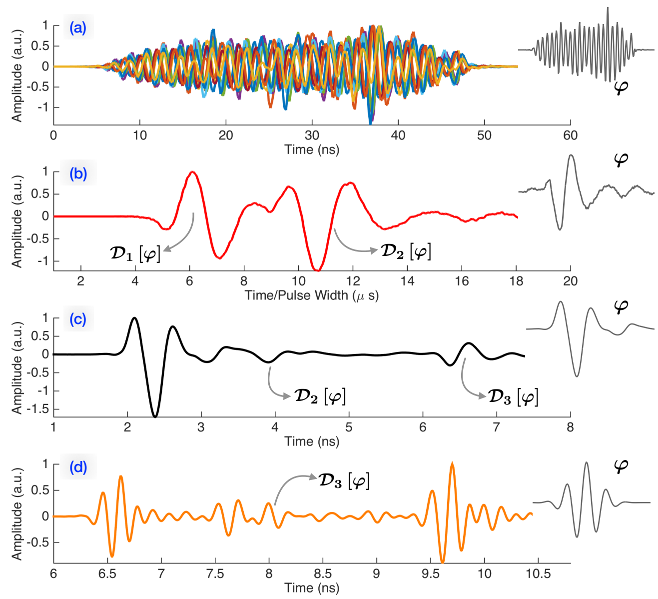

Fig. 1: Disparate case studies where the measurements are delayed, amplitude-scaled and distorted versions of the reference pulse φ shown in the inset. (a) Free electron laser measurements in Electron Paramagnetic Resonance. (b) Photoacoustic imaging. (c) Ground penetrating radar. (d) Ultra-wide band array.

where $\mathcal{L}$ is some invertible linear operator, such as a derivative or an integral and $\mathcal{L}[s]$ is specified by countable degrees of freedom.

Before the advent of high-resolution estimation methods [17], matched-filtering and cross-correlation operations were widely used for estimating $\{t_k\}$'s in (1). As a rule of thumb, whenever t_k's are sufficiently far apart (for instance, the Raleigh criterion is met), cross-correlation provides a reasonable estimate of the time delays. When the echoes are relatively close, FRI method may be used to super-resolve (cf. [18]). Be it something as simple as the cross-correlation or something more sophisticated, like the FRI, the estimation performance of the algorithms is heavily hindered by model mismatch. While the versatility of the FRI model (2) allows for representing a large class of signals, in a variety of problems, the model may take the form of,

$$y(t) = \sum\nolimits_{k=0}^{K-1} c_k \mathcal{D}_k[\varphi](t - t_k), \tag{3}$$

where $\mathcal{D}_k$ accounts for the time-varying distortion in pulse φ. Later, and with $c_k = |c_k| e^{\jmath \theta_k}, \varphi \in \mathbb{C}$, we will approximate (3) with,

$$y(t) \approx \sum\nolimits_{k=0}^{K-1} |c_k| \left(\cos\theta_k \, \varphi_{\mathsf{R}}(t - t_k) - \sin\theta_k \, \varphi_{\mathsf{I}}(t - t_k)\right).$$

We motivate this choice by considering the case studies that follow. In all of these cases, the measurements account for interaction of the reference pulse φ with a physical medium which results in shifted, amplitude-scaled and distorted versions of the reference pulse.

1.1. Case Studies Motivating Time-Varying FRI Sampling

1. Working in the area of Electron Paramagnetic Resonance (EPR) Edwards *et al.* [19] observe that the free electron laser (FEL) generated pulse is consistently distorted in connection with phase cycling. In view of (3), m^{th} laser pulse may be written as: $y_m(t) = c_m \mathcal{D}_m[\varphi](t)$. In Fig. 1(a), we plot the reference pulse φ as well as time aligned measurements $y_m(n\Delta), m = 1, \ldots, 10$.
2. Working in the area of photoacoustic imaging, Lee *et al.* [20] recently studied wave interference layered media. In view of (3), the transmitted and reflected waves are annotated as $\mathcal{D}_1[\varphi]$ and $\mathcal{D}_2[\varphi]$ in Fig. 1(b). Note the difference between $\mathcal{D}_1[\varphi]$ and φ.
3. Working in the area of ground penetrating radar (GPR), Safont *et al.* [21] study backscattered pulses from a historical wall with thickness 20 cm. Here we observe $K = 3$ echoes and $\mathcal{D}_3[\varphi]$ in Fig. 1(c) is associated with the back wall.
4. Working in the area of ultra-wide band (UWB) array based material identification, Maunder *et al.* [22] study reflected pulse properties for material classification and height estimation. Again, note the difference between $\mathcal{D}_3[\varphi]$ and φ.

From the examples above, it is clear that any attempt to explain the measurements with usual models discussed in literature [1–7] would be questionable due to significant model mismatch. Existing methods are based on:

Over-parametrization: One way to bypass model mismatch is to use over-parameterization (cf. 3.20, pg. 56 [23]),

$$\sum_{k=0}^{K-1} c_k \mathcal{D}_k[\varphi](t - t_k) \approx \sum_{k=0}^{K'-1} c'_k \varphi(t - t'_k),$$

where $K' > K$. However, this workaround may suffer from imprecise estimation of innovations $\{c_k, t_k\}$ which invariably stem from the physics of the problem. More precisely, going back to the example of GPR in Fig. 1(c), it may be hard to accurately measure the location as well as the thickness of the wall.

Model-based Fitting: Over-parametrization may implicitly be used in model based approaches [24, 25]. This class of methods use a parametric template $\varphi_{\mathbf{p}_k}(t) = \beta_k e^{-\lambda_k (t-\tau_k)^2} \cos(\omega_k (t - \tau_k) + \theta_k)$. Linear combination of basis functions $\varphi_{\mathbf{p}_k}(t)$ is used to fit the data with an unknown parameter vector $\mathbf{p}_k = [\beta_k \;\; \lambda_k \;\; \tau_k \;\; \omega_k \;\; \theta_k]$. Such methods are computationally intensive and a global minimum may not be guaranteed [25]. FRI based model-fitting for ECG was discussed in [26].

Minimum-phase Deconvolution Using kurtosis as a measure of sparsity, recently, Schmelzbach and Huber [27] proposed a decomposition of $\varphi = w_1 * w_2$ where w_2 is a minimum-phase filter and w_1 is some all-pass filter. Exact specification of sparsity can not be handled by such algorithms and reliable kurtosis estimation requires large sample size.

Blind Super-resolution: Letting $\mathcal{D}_k[\varphi] = \varphi_k$, Yang *et al.* [28] have recently proposed to simultaneously estimate $\{c_k, t_k, \varphi_k(n)\}_{k=0}^{K-1}$ assuming that $\{\varphi_k\}_{k=0}^{K-1}$ share a common, low-dimensional subspace. While this is certainly an interesting approach in the context of our problem, $\{\varphi_k\}_{k=0}^{K-1}$ may be agnostic to the physics of the problem.

Motivated by the case studies above, we setup the problem of FRI sampling with time-varying pulses. Unlike previous approaches, our work is based on the physical principles of time-varying phenomenon. In spirit of the FRI philosophy, our key contribution is to define the distortion with countable degrees of freedom. Experimental validation of our approach on all of the above mentioned case studies results in considerable gain in the peak-signal-to-noise ratio (PSNR), thus setting up a convincing case for much broader applicability of our work.

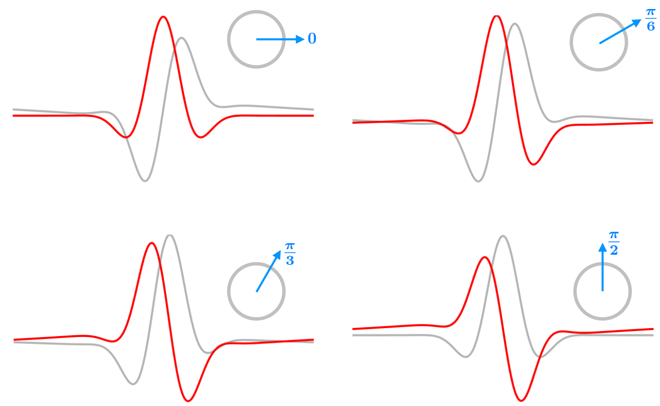

Fig. 2: We plot real (red) and imaginary (grey) parts of pulse $e^{\jmath\theta_k}\varphi(t), \theta_k = \pi k/6, k = 0, \ldots 4$ where φ is chosen to be a modulated Gaussian function (Gabor window) such that the real and imaginary parts from a quadrature pair.

2. PROBLEM FORMULATION

Wave propagation in a physical medium is a complex-valued phenomenon [19–22, 29] as opposed to the de-facto model assumptions in (1). Consequently, any inversion recipe pivoted on (1) (cf. [1–7] as well as [25, 27, 28]) fails to capture the underlying physics of reflection, transmission and scattering.

By design, all measurement devices capture real-valued information. Recovering complex-valued information given its real-valued proxy is an ill-posed problem. Let $z_0 \in \mathbb{C}$ be a complex number. A real-valued measurement is either obtained by the absolute operation ($|z_0|$) or the conjugate operation ($(z_0 + z_0^*)/2$). When dealing with absolute information, phase-retrieval algorithms are used for recovering the underlying complex-valued information. In our work, we focus on the second type of complex-to-real mapping.

2.1. The Forward Model

Letting φ and s to be complex-valued functions, we have,

$$y(t) = (s * \varphi)(t) = (y_{\mathsf{R}} + \jmath y_{\mathsf{I}})(t), \tag{4}$$

where the real and imaginary parts of y are,

$$y_{\mathsf{R}} = (s_{\mathsf{R}} * \varphi_{\mathsf{R}} - s_{\mathsf{I}} * \varphi_{\mathsf{I}}) \text{ and } y_{\mathsf{I}} = (s_{\mathsf{R}} * \varphi_{\mathsf{I}} + s_{\mathsf{I}} * \varphi_{\mathsf{R}}). \tag{5}$$

To this end, our complex-valued FRI signal representative of sparse reflectors/scatterers or response of layered media, may be modeled as,

$$s(t) = \sum_{k=0}^{K-1} c_k \delta(t - t_k), \quad c_k = |c_k| e^{\jmath\theta_k}. \tag{6}$$

With (5) and (6), real-valued sensor measurements are now explained by a linear combination of real and imaginary parts of s and φ, that is,

$$y_{\mathsf{R}}(t) = \sum_{k=0}^{K-1} |c_k| \left(\cos\theta_k \varphi_{\mathsf{R}}(t - t_k) - \sin\theta_k \varphi_{\mathsf{I}}(t - t_k)\right). \tag{7}$$

Consequently, the time-varying distortion $\mathcal{D}_k$ is explained as a combination of real and imaginary parts of the complex-valued pulse φ as shown in Fig. 2. The physical significance of complex-valued c_k lies in the interpretation of the Fresnel equations for reflection, refraction and transmission (cf. [30]). Next, we discuss how to estimate φ so that the innovations $\{c_k, t_k\}_k$ may be recovered from $y_{\mathsf{R}}(n\Delta)$.

Knowing φ is important for uniqueness of our representation. Independent of the context of discussion, the usual approach is to assume a parametric model for φ_{R} and fit it with some calibrated, real-valued pulse obtained experimentally [24, 25, 31]. Due to electro-optical and physical constraints of the measurement systems, it is reasonable to assume that φ is a smooth function [16, 18]. For this purpose, we resort to the idea that φ can reproduce upto M trigonometric moments,

$$\varphi(t) \approx \sum\nolimits_{m\in\mathbb{Z}} p_m e^{\jmath\omega_0 m t}, \tag{8}$$

where $\omega_0 = 2\pi/T$, $T = |t_K - t_0|$ assuming that $t_{k+1} > t_k$ and $p_m = 0, m \notin [0, M]$. In practice, this is a reasonably good choice for approximating φ. In fact, in many cases, it turns out that φ is a bandpass function. This is true of all the cases discussed in Section 1.1 (cf. [19–22] as well as ultrasound [24] and seismic imaging where wavelets are used. Keeping this bandpass nature of φ in mind, we will use,

$$p_m \equiv |p_m| e^{\jmath\xi_m} = 0, \quad m \notin [M_0, M_1], \quad M_0 > 0. \tag{9}$$

To give the reader an idea about the approximation using (8), in Fig. 3, we plot the real and imaginary parts of φ obtained via measurement together with its approximation (8) for the case study of GPR. The PSNR between the measurements and its approximation (8) was 40.68 dB.

2.2. Measurements

Note that property (9) in conjunction with (8) implies that φ_{R} and φ_{I} co-exist as a quadrature pair, that is, $\varphi_{\mathsf{I}} = \mathcal{H}[\varphi_{\mathsf{R}}]$ where $\mathcal{H}$ defines the Hilbert transform. This relation is of consequence to our work as it translates to the fact that the complex-valued measurements can be obtained from its real-valued counterparts.

Proposition 1 *Let $y \in \mathbb{C}$ be as defined in (5). Then, we have.*

$$\varphi_{\mathsf{I}} = \mathcal{H}[\varphi_{\mathsf{R}}] \Leftrightarrow y_{\mathsf{I}} = \mathcal{H}[y_{\mathsf{R}}].$$

Proof 1 The proof follows from two basic properties of the Hilbert transform. Let f and g be two given function, then, (1) Convolution: $\mathcal{H}[f * g] = \mathcal{H}[f] * g = \mathcal{H}[g] * f$ and, (2) Anti-involution: $\mathcal{H}[\mathcal{H}[f]] = -f$. ($\Rightarrow$) Let $\varphi_{\mathsf{I}} = \mathcal{H}[\varphi_{\mathsf{R}}]$ hold. Then, from (5),

$$\mathcal{H}[y_{\mathsf{R}}] = s_{\mathsf{R}} * \underbrace{\mathcal{H}[\varphi_{\mathsf{R}}]}_{=\varphi_{\mathsf{I}}} - s_{\mathsf{I}} * \underbrace{\mathcal{H}[\varphi_{\mathsf{I}}]}_{=-\varphi_{\mathsf{R}}} = y_{\mathsf{I}}.$$

Similarly, for ($\Leftarrow$), by letting $y_{\mathsf{I}} = \mathcal{H}[y_{\mathsf{R}}]$ we obtain the desired result.

Using this proposition, we can safely assume the knowledge of $y \in \mathbb{C}$,

$$\mathcal{C} : y_{\mathsf{R}} \to y = \mathcal{C}[y_{\mathsf{R}}] \stackrel{\text{def}}{=} y_{\mathsf{R}} + \jmath\mathcal{H}[y_{\mathsf{R}}], \tag{10}$$

provided that $\mathcal{H}[y_{\mathsf{R}}]$ can be accurately computed using continuous and sampled data. Given N–samples $y_{\mathsf{R}}(n\Delta)$, we first estimate the complex-valued vector of measurements $y \approx \mathcal{C}[y_{\mathsf{R}}](n\Delta)$ by using the discrete Hilbert transform. By using (8) and (6) in (4) the measurements in vector-matrix notation take form of:

$$y(n\Delta) = \sum\nolimits_{m=M_0}^{M_1} p_m \sum\nolimits_{k=0}^{K-1} c_k e^{\jmath\omega_0 m(n\Delta - t_k)} \Leftrightarrow \mathbf{y} = \mathbf{V}\mathbf{D}_p\widehat{\mathbf{s}} \tag{11}$$

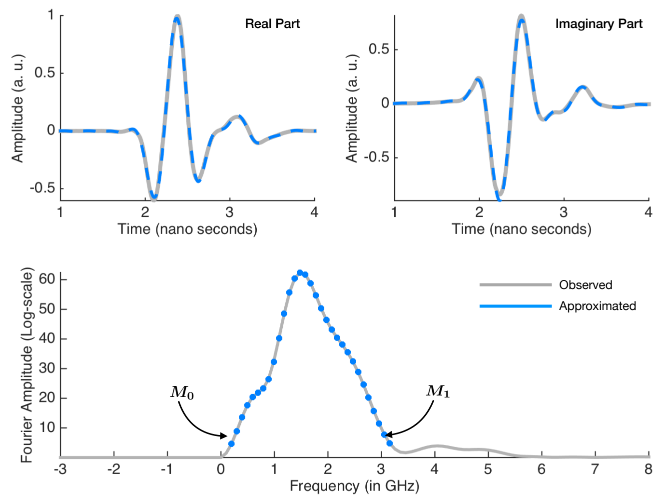

Fig. 3: Approximation of kernel used for ground penetrating radar experiment via finite Fourier series. The measured data is shown in grey ink. Dashed blue lines show its approximated version. Here $T = 10.14$ ns and $M_0 = 0.19$ GHz and $M_1 = 3.15$ GHz.

where,

- $\mathbf{y} \in \mathbb{C}^N$ is a vector of sampled measurements.
- $\mathbf{V} \in \mathbb{C}^{N\times(M_1-M_0+1)}$ is a DFT matrix with elements $\left[e^{\jmath m\omega_0 n\Delta}\right]_{n,m}$.
- $\mathbf{D}_p \in \mathbb{C}^{(\Omega\times\Omega)}$ is a diagonal matrix with diagonal elements p_m in (8). These are the Fourier-series coefficients of φ and $\Omega = M_1 - M_0 + 1$.
- $\widehat{\mathbf{s}} \in \mathbb{C}^{\Omega}$ is a vector of sampled Fourier transform of the FRI signal, that is, $\widehat{s}(\omega) = \sum_{k=0}^{K-1} c_k e^{-\jmath\omega_0 m t_k}, \omega = m\omega_0$.

2.3. Recovery Procedure

The first part of the recovery procedure relies on the usual FRI methodology. Given $\mathbf{y}$, we first estimate the vector of sum of complex exponentials. This is done by least-squares inversion of the linear system of equation in (11). More precisely, $\widehat{\mathbf{s}} = \mathbf{D}_p^{-1}\mathbf{V}^{+}\mathbf{y}$ where $(\cdot)^{+}$ denotes matrix pseudo-inverse. Having estimated $\widehat{\mathbf{s}}$, provided that $\Omega > 2K$, unknowns $\{t_k\}_{k=0}^{K-1}$ can be estimated using any of the spectral estimation methods [6, 7]. Nonetheless, complex-valued $\{c_k\}_{k=0}^{K-1}$ are estimated by relying on $\varphi = \varphi_{\mathsf{R}} + \jmath\mathcal{H}[\varphi_{\mathsf{R}}]$. For this purpose, we construct the matrix $\mathbf{\Phi} \in \mathbb{C}^{N\times K}$ with elements $\left[\varphi\left(n\Delta - \widetilde{t}_k\right)\right]_{n,k}$ where $\widetilde{t}_k$'s are the estimated innovations. Finally, we estimate, $\widetilde{\mathbf{c}} = \mathbf{\Phi}^{+}\mathbf{y}$.

3. EXPERIMENTAL VALIDATION

In the last decade, a number of papers have analyzed the performance of FRI methods. This has lead to interesting recoverability results [32] as well as robust algorithms for estimation of the innovations (cf. [33, 34] and references therein). Here, our goal is to establish the effectivity of the FRI model for time-varying pulses. Inspired by the case studies discussed in the introductory section, we will now demonstrate the flexibility of our proposed approach by revisiting each of those problems.

—• **Electron Paramagnetic Resonance** ($K = 1$) In [19], the authors acquire complex-valued pulses by recording $\sim$ 45 ns long pulses in quadrature. While the pulses are time-aligned, they are mismatched to the reference due to phase distortion (see Fig. 1(a)). Consider the m^{th} laser pulse measurements $y_{\mathsf{R}}^{(m)}(n\Delta), N = 4096, \Delta = 0.2$

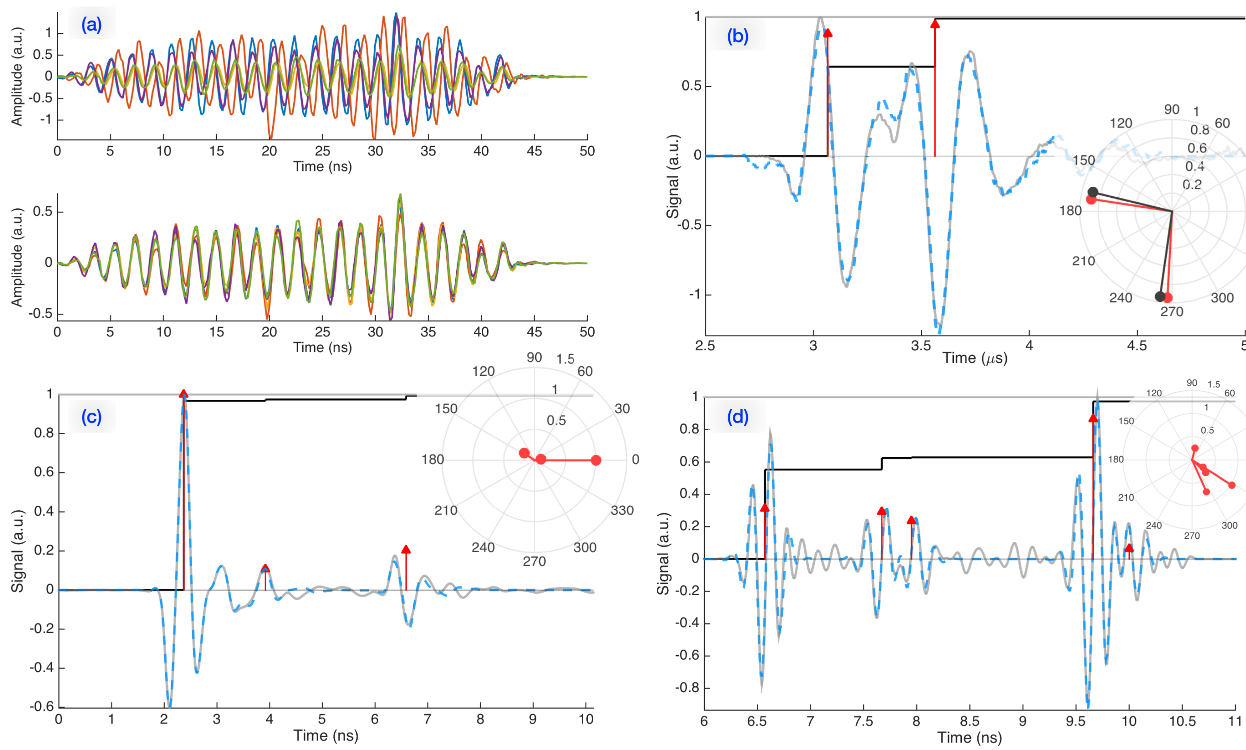

Fig. 4: With the exception of (a), for each case study we plot the measured data in grey ink, the reconstructed data in cyan ink and we mark the recovered spikes $\{|c_k|, t_k\}$ in ➝. The inset in each figure shows the polar-plot for $c_k \in \mathbb{C}$. In black ink, we plot the cumulative increase in ℓ_2-norm as each FRI component, that is, $|c_k| \cos\theta_k \varphi_{\mathsf{R}}(t - t_k)$ is added to reconstruction. Since the cumulative increase is relative to the ℓ_2–norm of y_{R}, when this value reaches 1, it implies that data is perfectly reconstructed. (a) Phase-distorted pulses together with FRI correction. (b) Time-varying pulse estimation in photoacoustic imaging. (c) Time-varying pulse estimation for thickness estimation in ground penetrating radar. (d) Time-varying pulse estimation in multi-layered UWB array.

ns. Given reference pulse, the FRI solution in this case is simply, $c_m\mathcal{C}[\varphi_{\mathsf{R}}]^{+}\mathcal{C}[y_{\mathsf{R}}^{(m)}]$. Experiments conducted with 14 realizations of pulses consistently validated the effectivity of our approach with an average enhancement of $\sim$ 8.65 db PSNR (when compared to the model in (1)). The results are plotted in Fig. 4(a).

Remaining experiments are based on the usual FRI setup and we use Cadzow's method as discussed in [7]. The kernel φ for each case is extracted from the data (cf. inset in Fig. 1). For the case of $K = 2$, we use exhaustive search to compare our method. For cases where $K > 2$, we rely on experimental settings for validation of our results.

—• **Two-pulse Experiment** ($K = 2$) In the context of photoacoustic imaging, we compare the performance of our method with exhaustive search. The experimental parameters are as follows: $N = 5003$, $\Delta = 1$ ns, $\Omega = 25$. Our method resulted in PSNR of 30.13 db compared to exhaustive search which resulted in 30.24 db. The error in estimation of $t_k, k = 1, 2$ was $0.003\mu s$ each. In the inset of Fig. 4(b), we compare c_k estimated from FRI method (red ink) with the result of exhaustive search (black ink). PSNR due to model (1) was 16.39 db. The results are plotted in Fig. 4(b).

—• **Backwall measurement** ($K = 3$) In context of ground penetrating radar, our method resulted in 35.84 db PSNR which was about 3.15 db higher when compared to (1). With $N = 1015$ samples and $\Delta = 10$ ps we used $\Omega = 25$ frequency samples for estimating $t_k = \{2.37 \;\; 3.92 \;\; 6.59\}$ ns. Given the speed of pulse in the material is $\nu = 92.56 \times 10^6$ m/s, the backwall echo with respect to the frontwall echo, that is $t_2 - t_0 = 4.22$ ns translates to $19.53 = (t_2 - t_0)/2\nu$ cm thickness. The ground truth thickness for this experiment was 20 cm [21]. The results are plotted in Fig. 4(c).

—• **UWB Material Classification** ($K = 5$) Our method resulted in 31.28 db PSNR which was about 9.3 db higher when compared to (1). With $N = 1799$ samples and $\Delta = 10$ ps we used $\Omega = 86$ frequency samples for estimating $t_k = \{6.57 \;\; 7.67 \;\; 7.95 \;\; 9.66 \;\; 10.00\}$ ns. Calibration of the antenna [22] suggested a reference offset of $t_c = 3.0$ ns. Estimation of t_k's are consistent with the experimental setup. For example, with $c = 3 \times 10^8$, $(t_0 - t_c)c/2$ translates to about half a meter which was the distance between the UWB antenna and the first reflector (cf. Table II, [22]). Furthermore, with $\varepsilon_1 = 2.5$ and $\varepsilon_2 = 8.4$, the estimates of height $h_1 = c(t_1 - t_0)/2\sqrt{\varepsilon_1} \approx 0.104$ m and $h_2 = c(t_3 - t_1)/2\sqrt{\varepsilon_2} \approx 0.103$ m are consistent with the experiments in [22]. The results are plotted in Fig. 4(d).

4. CONCLUSION

The problem of recovering spikes from time-varying pulses is discussed in this paper. For this purpose, we adapted the finite-rate-of-innovation signal model. The proposed approach was discussed in context of four case studies: (1) spectroscopy, (2) photo-acoustic imaging, (3) ground-penetrating radar and (4) ultra-wide band arrays. Our preliminary investigation demonstrates the effectivity of our proposed approach with a substantial boost in PSNR.

Acknowledgements The authors thank M. S. Sherwin, L. J. Guo, A. Salazar and P. Mousavi for discussing results and sharing data which has made this paper possible. Special thanks to Devin Edwards who went beyond the call of duty. Also, discussions with Taehwa Lee, Gonzalo Safont and Adam Maunder in context of the experimental setup are much appreciated.

5. REFERENCES

[1] J. Li and R. Wu, "An efficient algorithm for time delay estimation," *IEEE Trans. Signal Process.*, vol. 46, no. 8, pp. 2231–2235, Aug. 1998.

[2] A. Bruckstein, T.-J. Shan, and T. Kailath, "The resolution of overlapping echos," *IEEE Trans. Acoust., Speech, Signal Process.*, vol. 33, no. 6, pp. 1357–1367, Dec. 1985.

[3] Y. Bresler and A. H. Delaney, "Resolution of overlapping echoes of unknown shape," in *Proc. of IEEE ICASSP*, May 1989, pp. 2657–2660.

[4] L. Li and T. P. Speed, "Parametric deconvolution of positive spike trains," *Annals of Statistics*, pp. 1279–1301, 2000.

[5] E. Candès and C. Fernandez-Granda, "Towards a mathematical theory of super-resolution," *Commun. Pure Appl. Math.*, vol. 67, no. 6, pp. 906–956, 2014.

[6] M. Vetterli, P. Marziliano, and T. Blu, "Sampling signals with finite rate of innovation," *IEEE Trans. Signal Process.*, vol. 50, no. 6, pp. 1417–1428, 2002.

[7] T. Blu, P. L. Dragotti, M. Vetterli, P. Marziliano, and L. Coulot, "Sparse sampling of signal innovations," *IEEE Signal Processing Magazine*, vol. 25, no. 2, pp. 31–40, 2008.

[8] P. L. Dragotti, M. Vetterli, and T. Blu, "Sampling moments and reconstructing signals of finite rate of innovation: Shannon meets Strang–Fix," *IEEE Trans. Signal Process.*, vol. 55, no. 5, pp. 1741–1757, 2007.

[9] J. A. Urigüen, T. Blu, and P. L. Dragotti, "FRI sampling with arbitrary kernels," *IEEE Trans. Signal Process.*, vol. 61, no. 21, pp. 5310–5323, Nov. 2013.

[10] S. Deslauriers-Gauthier and P. Marziliano, "Sampling signals with a finite rate of innovation on the sphere," *IEEE Trans. Signal Process.*, vol. 61, no. 18, pp. 4552–4561, Sep. 2013.

[11] C. S. Seelamantula and S. Mulleti, "Super-resolution reconstruction in frequency-domain optical-coherence tomography using the finite-rate-of-innovation principle," *IEEE Trans. Signal Process.*, vol. 62, no. 19, pp. 5020–5029, Oct. 2014.

[12] Z. Doğan, T. Blu, and D. V. D. Ville, "Detecting spontaneous brain activity in functional magnetic resonance imaging using finite rate of innovation," in *IEEE Intl. Symp. on Biomed. Imaging*. IEEE, Apr. 2014.

[13] J. Murray-Bruce and P. L. Dragotti, "Estimating localized sources of diffusion fields using spatiotemporal sensor measurements," *IEEE Trans. Signal Process.*, vol. 63, no. 12, pp. 3018–3031, Jun. 2015.

[14] Y. Zhang and P. L. Dragotti, "Sampling streams of pulses with unknown shapes," *IEEE Trans. Signal Process.*, vol. 64, no. 20, pp. 5450–5465, Oct. 2016.

[15] A. Bhandari and Y. C. Eldar, "A swiss army knife for finite rate of innovation sampling theory," in *Proc. of IEEE ICASSP*, Mar. 2016, pp. 3999–4003.

[16] A. Bhandari and R. Raskar, "Signal processing for time-of-flight imaging sensors: An introduction to inverse problems in computational 3-D imaging," *IEEE Signal Processing Magazine*, vol. 33, no. 5, pp. 45–58, Sep. 2016.

[17] H. Zi-qiang and W. Zhen-dong, "A new method for high resolution estimation of time delay," in *Proc. of IEEE ICASSP*, vol. 7, May 1982, pp. 420–423.

[18] A. Bhandari, A. M. Wallace, and R. Raskar, "Super-resolved time-of-flight sensing via FRI sampling theory," in *Proc. of IEEE ICASSP*, Mar. 2016.

[19] D. T. Edwards, Y. Zhang, S. J. Glaser, S. Han, and M. S. Sherwin, "Phase cycling with a 240 GHz, free electron laser-powered electron paramagnetic resonance spectrometer," *Physical Chemistry Chemical Physics*, vol. 15, no. 15, p. 5707, 2013.

[20] T. Lee, Q. Li, and L. J. Guo, "Out-coupling of longitudinal photoacoustic pulses by mitigating the phase cancellation," *Nature Scientific Reports*, vol. 6, no. 21511, Feb. 2016.

[21] G. Safont, A. Salazar, A. Rodriguez, and L. Vergara, "On recovering missing ground penetrating radar traces by statistical interpolation methods," *Remote Sensing*, vol. 6, no. 8, pp. 7546–7565, Aug. 2014.

[22] A. Maunder and P. Mousavi, "Application of UWB arrays for material identification of multilayer media in metallic tanks," *IEEE Trans. Antennas Propag.*, vol. 63, no. 11, pp. 4901–4909, Nov. 2015.

[23] D. Asraf, "Optimal detectors for transient signal families and nonlinear sensors: Derivations and applications," Ph.D. dissertation, Uppsala University, 2003.

[24] R. Demirli and J. Saniie, "Model-based estimation of ultrasonic echoes. Part I: Analysis and algorithms," *IEEE Trans. Ultrason., Ferroelectr., Freq. Control*, vol. 48, no. 3, pp. 787–802, May 2001.

[25] F. Boßmann, G. Plonka, T. Peter, O. Nemitz, and T. Schmitte, "Sparse deconvolution methods for ultrasonic NDT," *J. Nondestr. Eval.*, vol. 31, no. 3, pp. 225–244, Apr. 2012.

[26] G. Baechler, N. Freris, R. F. Quick, and R. E. Crochiere, "Finite rate of innovation based modeling and compression of ECG signals," in *Proc. of IEEE ICASSP*. IEEE, May 2013.

[27] C. Schmelzbach and E. Huber, "Efficient deconvolution of ground-penetrating radar data," *IEEE Trans. Geosci. Remote Sens.*, vol. 53, no. 9, pp. 5209–5217, Sep. 2015.

[28] D. Yang, G. Tang, and M. Wakin, "Super-resolution of complex exponentials from modulations with unknown waveforms," *IEEE Trans. Inf. Theory*, pp. 1–1, 2016.

[29] L. Brekhovskikh, *Waves in Layered Media (second edition)*. Elsevier, 2012, vol. 16.

[30] M. Tygel and P. Hubral, "Transient analytic point-source response of a layered acoustic medium: Part I," *GEOPHYSICS*, vol. 50, no. 9, pp. 1466–1477, Sep. 1985.

[31] S. Hernandez-Marin, A. Wallace, and G. Gibson, "Bayesian analysis of lidar signals with multiple returns," *IEEE Trans. Pattern Anal. Mach. Intell.*, vol. 29, no. 12, pp. 2170–2180, Dec. 2007.

[32] X. Wei and P. L. Dragotti, "Guaranteed performance in the FRI setting," *IEEE Signal Process. Lett.*, vol. 22, no. 10, pp. 1661–1665, Oct. 2015.

[33] Z. Doğan, C. Gilliam, T. Blu, and D. V. D. Ville, "Reconstruction of finite rate of innovation signals with model-fitting approach," *IEEE Trans. Signal Process.*, vol. 63, no. 22, pp. 6024–6036, Nov. 2015.

[34] T. Michaeli and Y. C. Eldar, "Xampling at the rate of innovation," *IEEE Trans. Signal Process.*, vol. 60, no. 3, pp. 1121–1133, Mar. 2012.